doi:10.1111/evo.12956

EMMLi: A maximum likelihood approach to the analysis of modularity

Anjali Goswami[1,2,3] and John A. Finarelli[4,5,6]

[1]*Department of Genetics, Evolution and Environment, University College London, London WC1E 6BT, United Kingdom*

[2]*Department of Earth Sciences, University College London, London WC1E 6BT, United Kingdom*

[3]*E-mail: a.goswami@ucl.ac.uk*

[4]*School of Biology and Environmental Science, University College Dublin, Science Centre – West, Belfield, Dublin 4, Ireland*

[5]*UCD Earth Institute, University of College Dublin, Belfield, Dublin 4, Ireland*

[6]*E-mail: john.finarelli@ucd.ie*

Received June 18, 2015
Accepted May 7, 2016

Identification of phenotypic modules, semiautonomous sets of highly correlated traits, can be accomplished through exploratory (e.g., cluster analysis) or confirmatory approaches (e.g., RV coefficient analysis). Although statistically more robust, confirmatory approaches are generally unable to compare across different model structures. For example, RV coefficient analysis finds support for both two- and six-module models for the therian mammalian skull. Here, we present a maximum likelihood approach that takes into account model parameterization. We compare model log-likelihoods of trait correlation matrices using the finite-sample corrected Akaike Information Criterion, allowing for comparison of hypotheses across different model structures. Simulations varying model complexity and within- and between-module contrast demonstrate that this method correctly identifies model structure and parameters across a wide range of conditions. We further analyzed a dataset of 3-D data, consisting of 61 landmarks from 181 macaque (*Macaca fuscata*) skulls, distributed among five age categories, testing 31 models, including no modularity among the landmarks and various partitions of two, three, six, and eight modules. Our results clearly support a complex six-module model, with separate within- and intermodule correlations. Furthermore, this model was selected for all five age categories, demonstrating that this complex pattern of integration in the macaque skull appears early and is highly conserved throughout postnatal ontogeny. Subsampling analyses demonstrate that this method is robust to relatively low sample sizes, as is commonly encountered in rare or extinct taxa. This new approach allows for the direct comparison of models with different parameterizations, providing an important tool for the analysis of modularity across diverse systems.

KEY WORDS: **Mammals, model selection, phenotypic integration, trait correlations.**

The related topics of phenotypic integration and modularity, which concern associations among traits and their partitioning into semiautonomous and highly correlated subsets, respectively, have received increased attention over the past few decades as a powerful bridge among different scales of evolutionary analysis. Recent years have seen increasing effort to identify and compare phenotypic modularity and integration across taxa, in some cases spanning entire vertebrate "classes" (Goswami 2006a,b; Goswami 2007; Porto et al. 2009; Bell et al. 2011; Bennett and Goswami 2011; Klingenberg and Marugan-Lobon 2013), and even comparing plants and animals (Conner et al. 2014). There has also been a refining of different levels of modularity acting at different scales. The most typically studied level, termed "variational" (Marquez 2008) or "static" (Klingenberg 2014) modularity, focuses on a single species or population, commonly at a specific ontogenetic stage (e.g., adults). Within this level, analyses focus on identifying drivers of trait integration, whether functional, developmental, genetic, or environmental. Beyond variational modularity, studies have analyzed modularity at the ontogenetic (i.e., patterns or changes in modularity through ontogeny within a species), and evolutionary scales (comparative analysis of patterns of modularity across taxa). Coincident with this increase in studies

EVOLUTION
INTERNATIONAL JOURNAL OF ORGANIC EVOLUTION

of modularity, there has been an explosion in the number of methods proposed to analyze phenotypic modularity and integration, both within and across populations (Klingenberg 2009; Goswami and Polly 2010; Klingenberg 2013; Adams and Felice 2014; Bookstein and Mitteroecker 2014; Klingenberg 2014; Adams 2016).

Analyses of modularity have taken many forms, from entirely exploratory approaches, such as cluster analysis, Euclidean distance matrix analysis, and graphical modeling, to confirmatory approaches, such as partial least squares analysis and the related RV coefficient analysis, integration matrices, and theoretical matrix modeling (reviewed in Klingenberg 2009; Goswami and Polly 2010; Klingenberg 2013, 2014), and there has been a vigorous discussion of the merits, practical considerations, and issues of each approach (Klingenberg 2008; Goswami and Polly 2010; Fruciano et al. 2013; Adams and Felice 2014; Adams 2016). Not surprisingly, confirmatory methods are generally viewed as more robust, particularly as exploratory methods such as cluster analysis impose hierarchical relationships on traits that may or may not reflect their true biological organization. On the other hand, exploratory approaches have the benefit of not requiring a *priori* determination of model structure, whereas confirmatory methods depend on a defined model structure and are therefore limited to testing preselected models. Given the complexity of many biological structures, and the diverse factors that may influence trait relationships (Hallgrimsson et al. 2009), this limitation argues for the continued role of exploratory approaches, particularly as studies expand beyond well-established model systems. Recent work has developed relative eigenanalysis for the purpose of comparing two covariance matrices in a more informative manner than do previous methods, such as eigenvalue dispersion or random skewers analysis (Bookstein and Mitteroecker 2014), providing an efficient exploratory approach that can detail the specific ways that high-dimensional covariance matrices differ by identifying the maximal ratios of variance between any two groups. However, this approach does not directly address the problem of describing the pattern of integration for a group, which remains an outstanding issue in this field.

Another important issue with most current confirmatory approaches is that they are designed to measure support for alternative hypothesized parameter values within a proposed model structure (Wagner 2000). For example, RV coefficient analysis determines the correlations among sets of traits, and then randomizes trait associations to produce an empirical distribution of RV coefficients for the model structure under consideration, testing the hypothesis that the observed RV coefficient is significantly lower than random alternatives. But although this methodology can test if a particular model is more structured than random associations of traits, it does not readily address the question of whether a four-module model describes the pattern of phenotypic integration better than arrangements with three or five modules. The same is true of the recently described Covariance Ratio metric (Adams 2016), which improves upon several statistical issues with RV coefficient analysis, but also can only test one model of modularity against a hypothesis of random associations of traits. Thus far, only one published method allows for comparisons of models with different complexities (Marquez 2008), as demonstrated with a 2-D landmark dataset for rodent mandibles. This method included several innovations that allowed for testing of hundreds of alternative models, including those with overlapping landmarks, but the most relevant is the correction of similarity among the observed and modeled covariance matrices against the number of estimated parameters. This addition facilitates comparison across models with varying structures of different complexity. Although this method represented an important step in confirmatory tests of modularity, the author noted that a linear correction for the number of estimated parameters may not be appropriate for all test statistics or for more complex approaches (Marquez 2008). Additionally, this method has also never been expanded to 3-D data.

Here, we describe a new method for the analysis of phenotypic modularity from trait correlation matrices based on a maximum likelihood approach. We provide a case study applying this approach to a dataset of macaque skulls spanning infant to adult age groups. We use this method to compare various models that have been proposed for mammalian skull modularity (including no modularity, a two-module neurocranial/facial hypothesis, and multiple six-module hypotheses; Fig. 1), as well as novel alternative models of varying structure and complexity.

EMMLi: Evaluating Modularity with Maximum Likelihood

Model selection approaches using information theory compare likelihood fits across a set of models of varying degree of complexity. To estimate likelihoods of models of trait integrations, we first model the expected distribution around a hypothesized value representing the relationship among a set of traits. For the product moment correlation coefficient, and its derivatives including the congruence coefficient and canonical correlation (Goswami and Polly 2010), a simple transformation is available in the Fisher *r*–*z* transformation:

$$z_r = \boldsymbol{tanh}^{-1}(\boldsymbol{r}) = \frac{1}{2}\ln\left(\frac{1+\boldsymbol{r}}{1-\boldsymbol{r}}\right) \text{ (Sokal and Rohlf 1995, p. 575),} \quad (1)$$

where r is the sample correlation coefficient. Here, the observed correlation matrix is treated as a set of realizations (the values

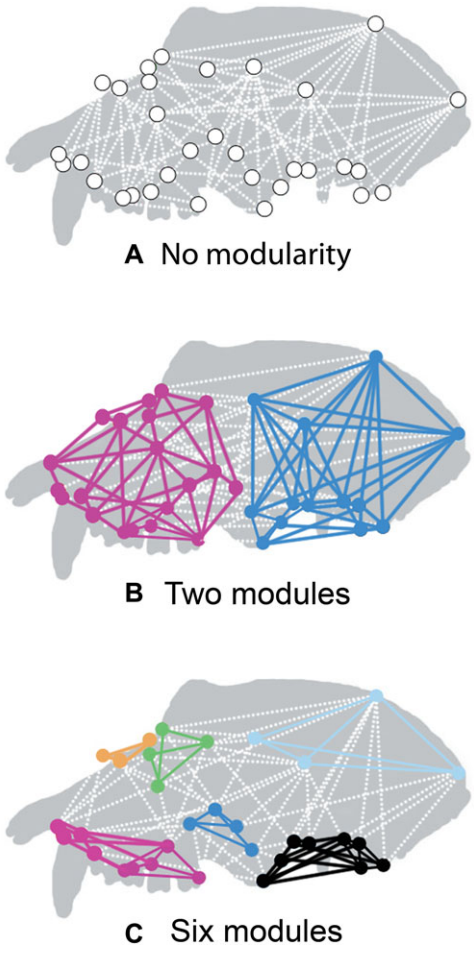

Figure 1. Schematic depiction of three alternative partitions of the macaque cranium. (A) No modularity, with similar levels of correlation among all landmarks. (B) Two modules, corresponding to facial and neurocranial regions. (C) Six modules, corresponding approximately to Cheverud's model (1982). Colored circles indicate module associations. Solid lines indicate within-module correlations. Dotted lines indicate between-module correlations.

of r) of a hypothesized true correlation coefficient (ρ). The distribution around a hypothesized value of ρ is approximately normally distributed with parameters:

$$\mu_\rho = z_\rho = \frac{1}{2}\ln\left(\frac{1+\rho}{1-\rho}\right) \quad (2a)$$

and

$$\sigma_\rho{}^2 = \left(\frac{1}{\sqrt{n-3}}\right)^2 = \frac{1}{n-3} \text{ (Sokal and Rohlf 1995, p. 575),} \quad (2b)$$

where n is the sample size used to calculate the correlation coefficient (i.e., the number of specimens with measured landmarks).

The log-likelihood support for a hypothesized value of ρ, given an observed value of r, is then:

$$LogL \propto -\frac{1}{2}Ln\left(\sigma_\rho{}^2\right) - \frac{\left(z_r - \mu_\rho\right)^2}{2\sigma_\rho{}^2} \text{ (Edwards 1992).} \quad (3)$$

Applying equation (3) to a matrix of trait correlations, the simplest model structure (no modularity) proposes a single value for the correlation coefficient between all possible trait pairs. The value that maximizes the summed log-likelihood for all observed correlations in the matrix would then be the preferred hypothesis, and this log-likelihood would then be the model log-likelihood for the "no modularity" model structure.

However, given the results of a large number of previous studies (Cheverud 1982, 1989, 1995, 1996; Ackermann and Cheverud 2000; Marroig and Cheverud 2001; Hallgrimsson et al. 2004; Goswami 2006a; Hallgrimsson et al. 2009; Porto et al. 2009; Goswami and Polly 2010; Klingenberg 2013), it is highly likely that a model structure positing a single value of ρ for the entire correlation matrix would not adequately describe trait correlations in a real biological system. Model structures of varying complexity can be compared using the Akaike Information Criterion (AIC; Akaike 1973; Burnham and Anderson 2002), assessing the likelihood fit of the models, while controlling for better fit induced by increased model complexity. The finite-sample AIC (AIC_c) is given by:

$$AIC_c = -2LogL + 2K + \frac{2K\ (K+1)}{N-K-1} \text{ (Hurvich and Tsai 1989).} \quad (4)$$

In equation (4), N is the sample size, but in the case of computing AIC_c, this is the number of between-trait correlations used to calculate the likelihood score. K is the number of estimated parameters, which is the number of distinct, optimal correlations estimated by the model, and an additional parameter for each estimate of the variance around the hypothetical value of ρ (see eq. 2b). In the present analysis, this is fixed for all of the examined models within each dataset (a single variance was calculated for each dataset based on its sample size), and the number of parameters is simply the number of estimated values of ρ incremented by one for all models. However, this does not need to be the case, as more complex analyses may wish to consider whether patterns of modularity are common across multiple datasets, which may have different estimates of variance. In such cases, different variances may be included as estimated parameters among different models.

To illustrate the designation of model parameters more clearly, consider a set of landmarks across a mammal cranium (Fig. 2A). Previous study of the mammal skull has proposed six

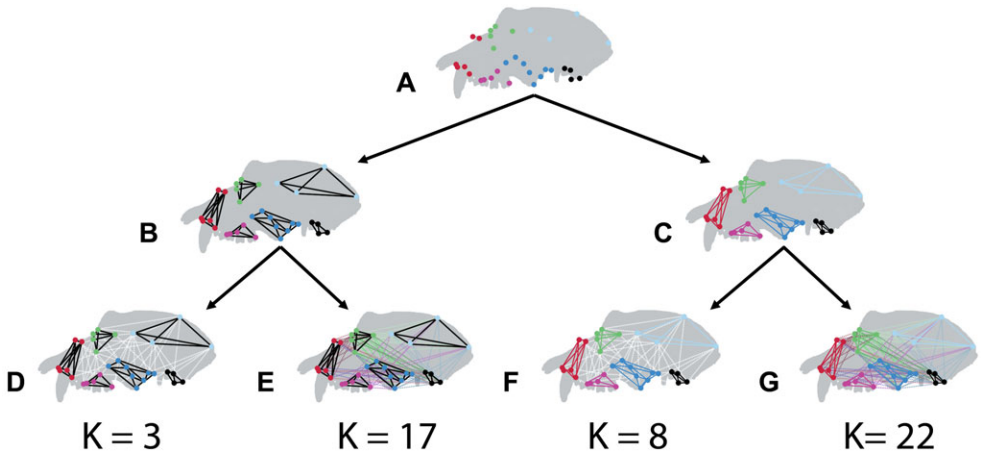

Figure 2. Schematic depiction of the four alternative parameterizations of a single six-module model structure. (A) Basic structure of landmark associations in six modules, indicated by colors. The six modules may have either similar (B) or different (C) magnitudes of within-module correlations. The intermodule correlations may also be similar (D and F) or different (E and G) among all pairs of modules. Each distinct estimated value of ρ is counted as a parameter, along with one additional parameter for estimated variance. Solid lines indicate within-module correlations. Dashed lines indicate between-module correlations. Line colors indicate similar or different estimated values for ρ (e.g., in (B), the black lines indicate that all of the six modules have the same estimated within-module correlation).

modules for this system (Cheverud 1982; Goswami 2006a). It is possible that the magnitudes of within-module correlations are effectively the same in all of the modules (Fig. 2B) or that each of these modules has distinct strengths of correlation between landmarks within a given module (Fig. 2C). Furthermore, intermodule correlations could also be distinct for each module-to-module set (Fig. 2E and G), or they could be effectively identical (Fig. 2D and F). These variations then return four potential model structures with three, 17, eight, or 22 estimated parameters (the number of estimated ρ′s in each, plus one for the estimated variance). Summing the log-likelihoods from equation (3) for the set of observed correlations within each modeled set for an optimal estimate of ρ, gives the model log-likelihood. These log-likelihoods can be compared to one another, to the "no modularity" hypothesis, and to different proposed structures or different groupings of the landmarks within modules using equation (4). From the model AIC_c scores, we calculate ΔAIC_c, the difference between a particular model's AIC_c score and the lowest score observed among the tested models. From this, we calculate the model log-likelihood adjusting for the penalty due to parameterization:

$$\textbf{\textit{Model LogL}} \propto -\frac{1}{2}\Delta \textbf{\textit{AIC}}_{\mathbf{c}} \text{ (Burnham and Anderson 2002).} \quad (5)$$

A set of model posterior probabilities can then be calculated by dividing each model's likelihood by the sum of likelihoods over the set of examined models (NB these are likelihoods, and are therefore equal to $e^{\text{Model LogL}}$ (see Burnham and Anderson 2004).

A NOTE ON SAMPLE SIZE

A value of "*n*" or sample size appears in both the equations for calculating the variance around an estimated value of ρ (eq. 2b) and for the calculation of the AIC statistic (eq. 5). We have used upper- and lowercase to distinguish between the two, as *n* for calculation of correlations is based on the number of specimens, whereas, in the case of computing AIC_c, *N* is the number of between-trait correlations considered in calculating the log-likelihood. For a 61 landmark data matrix, there are 1830 unique between-landmark correlations (i.e., the subdiagonal values of the matrix).

A NOTE ON THE USE OF THE FISHER TRANSFORMATION

The Fisher *r*–*z* Transformation converts the bounded correlation coefficient to an unbounded variable. Comparison of the transformed correlation to a hypothetical population value of ρ demonstrates that the transformed coefficient is approximately normally distributed about ρ, making the Fisher Transformation attractive for hypothesis testing. In the case of the correlation matrix, however, there is a concern about the independence of the sample of correlation coefficients, in that, for example, elements r_{12} and r_{13} are not strictly random *iid* draws from a population, but are themselves intercorrelated. However, the Fisher-transformed correlations within a correlation matrix have been shown to be asymptotically, multivariate normal in distribution, and robust to the violations of independence (Steiger 1980b; De Leeuw 1983). Specifically, this has been demonstrated for pattern hypotheses within correlation matrices, wherein observed correlation coefficients are tested against a proposed "pattern matrix" (Steiger 1980a), and this approach, which is adopted here in the form of

the proposed within- and among- module correlation estimates, has been applied in a wide range of research questions (Feldman et al. 2007; Wager et al. 2007; LeBel and Gawronski 2009). As such the employing Fisher-transformed correlations in a likelihood framework, as proposed here, should prove a reliable approach to evaluating modularity with trait correlation matrices.

Simulations

Given the above-noted concern with respect to independence of the Fisher-transformed correlation coefficients, we evaluated the ability of the maximum likelihood approach as implemented in EMMLi to correctly select a known model when choosing among models structures. To do so, we conducted an extensive series of simulations testing a range of model structures, contrasting two variables: model complexity (number of parameters) and contrast (difference between within-module and between-module strength of integration). In all cases, 60 "landmarks" were simulated as divided into zero, two or six modules, to represent a hypothetical correlation structure that we wish to evaluate. Between-module correlations were set at a mean value of 0.1 for all simulations. SDs for generating correlations were varied from a low value of $\sigma = 0.01$ to realistic value of $\sigma = 0.05$ (e.g., Cheverud 1982), encompassing values used in simulations testing other recently described methods for the analysis of modularity (Adams 2016).

Simulating datasets without any modular structure allowed for assessment of Type I error rates. One hundred permutations each were run with the mean correlations among all traits simulated as $r = 0.15$, 0.3, 0.5, 0.7, or 0.9, with $\sigma = 0.01$ or 0.05, for a total of 1000 simulations. In these cases, the correct model would be equivalent in structure to model 1 ($K = 2$) in Table 1.

For the two and six module structures, both simple and complex models were tested. The simple models involved two or six modules, which all had the same within-module correlations, set to five mean values ranging from $r = 0.15$ in the lowest contrast model to $r = 0.9$ in the highest contrast model (i.e., mean within-module $r = 0.15$, 0.3, 0.5, 0.7, and 0.9 were all simulated).

For the complex models, all two or six modules had different within-module correlations. In the high contrast, complex two-module model, these values were set to mean within-module $r = 0.7$ and 0.9; in the mixed contrast model, mean within-module $r = 0.3$ and 0.8; and in the low contrast case, mean within-module $r = 0.15$ and 0.3. In the high contrast, complex six-module model, mean within-module $r = 0.7$, 0.75, 0.8, 0.85, 0.9, and 0.95; in the mixed contrast case, mean within-module $r = 0.3$, 0.4, 0.5, 0.6, 0.7, and 0.8; and in the low contrast case, mean within-module $r = 0.15$, 0.2, 0.25, 0.3, 0.35, and 0.4. For the simple two-module structure, the correct model would be equivalent in structure to model 2 ($K = 3$) in Table 1, and the complex structure would be equivalent to model 3 ($K = 4$). For the simple six-module structure, the correct model would be equivalent in structure to model 4 or 8 ($K = 3$) in Table 1, and the complex structure would be equivalent to model 5 or 9 ($K = 8$). One hundred permutations each of these 16 models were run, using each of the SD levels, resulting in 3200 total simulations of these modular structures.

Case Study: Maximum Likelihood Analysis of Macaque Cranial Modularity

MATERIALS

We used a dataset of 3-D coordinates for 61 landmarks taken on the cranium of Japanese macaque (*Macaca fuscata*) from the Primate Research Institute at Inuyama, Japan, previously described in Goswami and Polly (2010; see Supporting Information). Individuals were divided into five datasets representing four age classes: infants with deciduous dentition only ($n = 42$), juveniles with M1 erupted ($n = 42$), subadult with M2 erupted ($n = 48$), and adults with the entire adult dentition, with adults further divided into male and female data partitions ($n_m = 25$, $n_f = 24$). See Goswami and Polly (2010) for further details on the dataset used in the following analyses.

The landmark data were superimposed with Generalized Procrustes superimposition to remove the effects of rotation, translation, and size (scaling all specimens to unit centroid size). All five datasets were analyzed separately. We calculated vector congruence coefficient correlation matrices, producing 61×61 element matrices. This vector-based approach allows for simultaneous analysis of all three coordinates representing a single landmark (Goswami 2006a; Goswami and Polly 2010). There has been some debate about the use of vector-based versus coordinate-based correlations in studies of phenotypic integration and modularity (Klingenberg 2008; Goswami and Polly 2010; Klingenberg 2013). Here, we used the vector-based matrices, as we feel these better reflect biological relationships, treating each landmark as a single unit of information. However, we also included an example using the correlation matrix for individual coordinates for the M1-erupted dataset (see Supporting Information). This is a 183×183 matrix (x-, y- and z-coordinates for each of 61 landmarks). We used the absolute values of correlations in all analyses, as the magnitude of correlation, rather than its direction, is the unit of interest in studies of integration and modularity. Allometric effects and asymmetric variation have not been removed from the example dataset, for comparability with previously published analyses of macaque skull modularity (Cheverud 1982; Goswami and Polly 2010), although, as with selection of metric of trait correlation, the model presented here is applicable to datasets that do remove, or focus entirely on, those aspects of shape.

Table 1. Model descriptions and parameterizations for the 31 model structures explored in this study.

Model ID	Base model structure	# Modules	Model description	# Parameters
1	No modules	0	One ρ for all correlations	2
2	Neurocranial/Facial model	2	One within module ρ for both modules, one between-module ρ	3
3	Neurocranial/Facial model	2	Two within-module ρs and one between-module ρ	4
4	Cheverud model	6	One within-module ρ and one between-module ρ	3
5	Cheverud model	6	Separate within-module ρs and one between-module ρ	8
6	Cheverud model	6	One within-module ρ and separate between-module ρs	17
7	Cheverud model	6	Separate within-module ρs and separate between-module ρs	22
8	Goswami model	6	One within-module ρ and one between-module ρ	3
9	Goswami model	6	Separate within-module ρs and one between-module ρ	8
10	Goswami model	6	One within-module ρ and separate between-module ρs	17
11	Goswami model	6	Separate within-module ρs and separate between-module ρs	22
12	Cheverud/Goswami combined model	8	One within-module ρ and one between-module ρ	3
13	Cheverud/Goswami combined model	8	Separate within-module ρs and one between-module ρ	10
14	Cheverud/Goswami combined model	8	One within-module ρ and separate between-module ρs	30
15	Cheverud/Goswami combined model	8	Separate within-module ρs and separate between-module ρs	37
16	Tissue Origin model	3	One within-module ρ and one between-module ρ	3
17	Tissue Origin model	3	One within-module ρ and separate between-module ρs	5
18	Tissue Origin model	3	Separate within-module ρ and one between-module ρs	5
19	Tissue Origin model	3	Separate within-module ρ and separate between-module ρs	7
20	Cheverud-based "monotreme" model	3	One within-module ρ (for modules 1, 2, and 6 only), one pooled between-module and unintegrated ρ	3
21	Cheverud-based "monotreme" model	3	One within-module ρ (for modules 1, 2, and 6 only), one between-module ρ, and one unintegrated ρ	4
22	Cheverud-based "monotreme" model	3	Separate within-module ρs (for modules 1, 2, and 6 only), one pooled between-module and unintegrated ρ	5
23	Cheverud-based "monotreme" model	3	Separate within-module ρs (for modules 1, 2, and 6 only), one between-module ρ, and one unintegrated ρ	6
24	Cheverud-based "monotreme" model	3	One within-module ρ (for modules 1, 2, and 6 only), separate between-module ρs, and one unintegrated ρ	6

(Continued)

Table 1. Continued.

Model ID	Base model structure	# Modules	Model description	# Parameters
25	Cheverud-based "monotreme" model	3	Separate within-module ρs (for modules 1, 2, and 6 only), separate between-module ρs, and one unintegrated ρ	8
26	Goswami-based "monotreme" model	3	One within-module ρ (for modules 1, 2, and 6 only), one pooled between-module and unintegrated ρ	3
27	Goswami-based "monotreme" model	3	One within-module ρ (for modules 1, 2, and 6 only), one between-module ρ, and one unintegrated ρ	4
28	Goswami-based "monotreme" model	3	Separate within-module ρs (for modules 1, 2, and 6 only), one pooled between-module and unintegrated ρ	5
29	Goswami-based "monotreme" model	3	Separate within-module ρs (for modules 1, 2, and 6 only), one between-module ρ, and one unintegrated ρ	6
30	Goswami-based "monotreme" model	3	One within-module ρ (for modules 1, 2, and 6 only), separate between-module ρs, and one unintegrated ρ	6
31	Goswami-based "monotreme" model	3	Separate within-module ρs (for modules 1, 2, and 6 only), separate between-module ρs, and one unintegrated ρ	8

Base models structures follow the allocation of landmark variables in Table S1. Model parameters are a sum of the number of estimated correlations within modules and across modules, plus one (for the estimate of the variance of the population correlation).

MODELS

We investigated 31 model structures within several broad hypotheses of cranial modularity. The first, and simplest, model structure is that there are no distinct modules within the cranium, and that the cranium can be analyzed as a single entity. Further, more complex models of modularity consist of a two-module (neurocranial vs. facial) structure (Drake and Klingenberg 2010), two six-module structures (primate-specific (Cheverud 1995) and general mammalian (Goswami 2006a)), and an eight-module structure combining the two six-module models (see Table S1). We investigated further refinements for both configurations of the six-module structure: first, leaving some landmarks "unintegrated," that is, outside of any module, based on a monotreme model of integration (Goswami 2006a), resulting in three-module + "unintegrated" models; and, second, considering a tissue-origin model (Goswami 2006a), in which landmarks were grouped based on their derivation from neural crest, mesodermal, or mixed germ layer-derived bone (see Table S1).

As detailed above, each hypothesized model structure may have many potential parameterizations, depending on whether within-module or across-module correlations are modeled as being the same for all cases (e.g., a single hypothesized correlation within modules and a single, across-module correlation), or all module cases are considered unique, or some mixture of these extremes. For example, the two-module neurocranial/facial model structure comprises Models 2 and 3 (Table 1), with the difference being the number of proposed within-module estimates. Models with increasing numbers of modules have correspondingly greater complexity in their potential parameterizations. As described above, the six-module model has four different parameterizations examined here (Fig. 2). In the simplest model (Model 4, Fig. 2D), there is a single within-module estimate and a single across-module estimate. Other models propose six freely varying within-module estimates with a constant across-module estimate (Model 5, Fig. 2F), 15 freely varying across-module estimates with a single within-module estimate (Model 6, Fig. 2E) and a completely varying model with six within-module estimates and 15 across-module estimates (Model 7, Fig. 2G). All model structures that were explored and their corresponding parameterizations are given in Table 1. The R code used in this analysis and example data files are provided in the online supporting information for this article and are available for download from: http://www.goswamilab.com/#!software/c1cxq.

SUBSAMPLING ANALYSIS

Although analyses of integration are often performed on model systems with the ability to sample large numbers of individuals, questions about the evolution of integration can require the

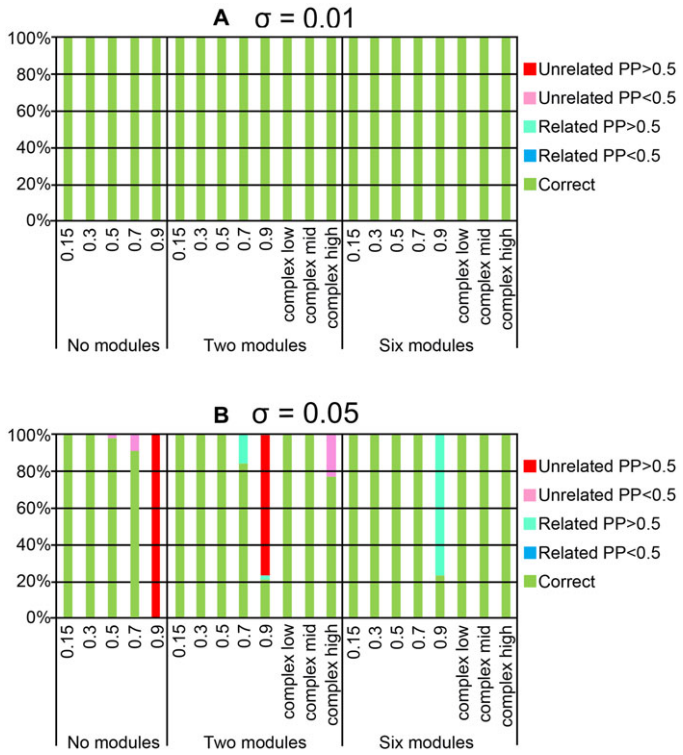

Figure 3. **Results of simulations demonstrating accuracy in model selection for different model structures (no modularity, two modules, or six modules), complexity (similar or different within-module correlations), and magnitudes of within-module correlations, modeled with varying SDs of (A) σ = 0.01 or (B) σ = 0.05. Stacked bars show percentage of simulations identifying: the correct model (green), an alternative parameterization of the same model structure, that is, a related model, with posterior probability < 0.50 (dark blue), a related model with posterior probability > 0.50 (light blue), an unrelated model with posterior probability < 0.50 (pink), or an unrelated model with posterior probability > 0.50 (red). Simulated mean within-module correlations, or all correlations for no modularity models, are indicated on the x-axis. Hundred simulations were run for each model, resulting in a total of 4200 simulations. Results show that this method is highly accurate at identifying the correct model structure, except where higher SDs are combined with extremely high correlations and simple model structures (no modularity, in particular).**

incorporation of fossil or rare taxa (Goswami et al. 2015) for which sample sizes are constrained. To evaluate potential sensitivity of this method to small sample sizes, we conducted a subsampling analysis of the best sampled dataset (subadult *Macaca*, 48 specimens), producing 50 random subsets each of 25 specimens, 15 specimens, and 10 specimens. Each subset was subjected to generalized Procrustes analysis prior to calculation of vector congruence coefficient correlation matrices, producing 61 × 61 element matrices, and analyzed in EMMLi.

Results

SIMULATIONS

When a low SD ($\sigma = 0.01$) around the simulated correlation values was used, the correct model structure was identified as the best fit model in 100% of cases for all no-module, two-module, and six-module structures (Fig. 3A). Reconstructed ρ values were consistently within 0.01 of the simulated values. For the simulations of a no-modularity dataset, posterior probabilities were generally low, ~0.24, even for the best fit model. All posterior probabilities for the correct model were >0.5 for the simulations in which there was a modular structure to the data. In all cases, estimated ρ values exactly matched those used to generate the simulated datasets.

When a higher SD of 0.05 was used, the correct model was identified in most cases, although accuracy decreased at the highest levels of mean correlations for simple structures (Fig. 3B). The correct model was selected with high (>0.90) posterior probability in 100% of cases for the simple six-module model with within-module correlations ranging from 0.15 to 0.70. It was also correct, with 100% posterior probability, in all cases for the complex six-module structure, using either high, mixed, or low correlations. When all within-module correlations were set to 0.90 (simple six-module model), the correct model was selected in 23 of 100 runs, and receives a posterior probability > 0.05 in 36 of 100 runs, with a different parameterization of the same model structure (six modules, $K = 8$) selected in all remaining cases. For the two-module model, the correct model was selected in 100% of cases

Table 2. Results for the Subadult (M2 erupted) dataset ($n = 48$) using congruence coefficients.

Model ID	K	LogL	AIC_c	ΔAIC_c	Model LogL	Model posterior probability
1	2	2078.86	−4153.72	916.21	1.11E-199	1.11E-199
2	3	2134.49	−4262.97	806.96	5.89E-176	5.89E-176
3	4	2147.54	−4287.06	782.88	1.00E-170	1.00E-170
4	3	2219.34	−4432.67	637.26	4.17E-139	4.17E-139
5	8	2380.83	−4745.58	324.35	3.69E-71	3.69E-71
6	17	2395.76	−4757.18	312.75	1.22E-68	1.22E-68
7	***22***	***2557.25***	***−5069.93***	***0.00***	***1.00***	***1.000***
8	3	2153.94	−4301.87	768.06	1.65E-167	1.65E-167
9	8	2226.56	−4437.03	632.90	3.69E-138	3.69E-138
10	17	2257.63	−4480.93	589.01	1.26E-128	1.26E-128
11	22	2330.25	−4615.93	454.00	2.60E-99	2.60E-99
12	3	2172.35	−4338.69	731.24	1.63E-159	1.63E-159
13	10	2246.04	−4471.95	597.98	1.41E-130	1.41E-130
14	30	2417.44	−4773.85	296.09	5.07E-65	5.07E-65
15	37	2491.12	−4906.68	163.26	3.54E-36	3.54E-36
16	3	2079.47	−4152.93	917.00	7.50E-200	7.50E-200
17	5	2214.56	−4419.08	650.85	4.67E-142	4.67E-142
18	5	2109.73	−4209.43	860.51	1.39E-187	1.39E-187
19	7	2244.82	−4475.57	594.36	8.62E-130	8.62E-130
20	3	2262.47	−4518.93	551.01	2.24E-120	2.24E-120
21	4	2265.54	−4523.05	546.88	1.76E-119	1.76E-119
22	5	2324.39	−4638.75	431.18	2.34E-94	2.34E-94
23	6	2327.46	−4642.87	427.06	1.84E-93	1.84E-93
24	6	2286.11	−4560.17	509.76	2.03E-111	2.03E-111
25	8	2348.03	−4679.99	389.95	2.11E-85	2.11E-85
26	3	2181.12	−4356.23	713.70	1.05E-155	1.05E-155
27	4	2181.12	−4354.23	715.71	3.85E-156	3.85E-156
28	5	2204.15	−4398.27	671.66	1.42E-146	1.42E-146
29	6	2204.15	−4396.26	673.67	5.17E-147	5.17E-147
30	6	2195.90	−4379.76	690.18	1.35E-150	1.35E-150
31	8	2218.93	−4421.78	648.15	1.80E-141	1.80E-141

Model parameters, raw log-likelihood fits for each tested model, AIC_c and ΔAIC_c scores are provided. Model log-likelihoods and the model posterior probability are also shown. Sample size used to calculate AIC_c was 1830. See methods for details. Model ID's correspond to the numbering in Table 1. The optimal model in the set of evaluated models is highlighted in bold italics.

for within-module correlations of 0.15, 0.30, and 0.50. The correct model is selected in 84 of 100 cases when the within-module correlation is 0.70, and receives a posterior probability > 0.05 in 100% of cases. In the remaining 16 runs, the closely related, more parameterized two-model model ($K = 3$) was selected as the best fit model. When within-module correlations are centered around 0.90, an unrelated model was selected in the majority of cases. The correct model was selected in 100% of cases with the complex two-module model using low or mixed correlations. When only the highest correlations (0.70 and 0.90) were used to simulate a complex two-module structure, the correct model was selected in 77 of 100 cases and had a posterior probability > 0.05 in 83 of 100 cases.

The strongest effects of high correlations and higher SD were observed in cases of no modularity in the simulated structure (Fig. 3B). The correct model was selected in 100% of cases when the overall correlation was 0.15 or 0.30. When the overall correlation was 0.50, the correct model was selected as the best fit model in 98 of 100 runs and had a posterior probability > 0.05 in all runs. With overall correlations of 0.70, the correct model was selected as the best fit model in 53 of 100 cases and had a posterior probability > 0.05 in 95 cases. In the cases where the wrong model was selected, the posterior probability was < 0.50 in all but five cases, although, as noted above, posterior probabilities are generally low ($\sim$0.2) for models of no modularity, even when the correct model was selected. When the overall correlation was extremely high, 0.90, the wrong model was selected with posterior probability > 0.50 in all runs. Even in cases where the wrong model was supported, estimated ρ values were within 0.03 of the values used to simulate each dataset.

Table 3. Optimal values of ρ within the six modules and for the 15 intermodule correlations estimated in Model 7 for each of the macaque datasets, partitioned by ontogenetic stage.

	Adult Females	Adult Males	Subadult (M2 erupted)	Juvenile (M1 erupted)	Infant (Deciduous only)
Module 1	0.43	0.46	0.43	0.44	0.55
Module 2	0.77	0.77	0.81	0.76	0.67
Module 3	0.24	0.35	0.40	0.19	0.22
Module 4	0.15	0.18	0.14	0.16	0.15
Module 5	0.12	0.23	0.14	0.17	0.23
Module 6	0.28	0.29	0.30	0.30	0.28
M1–M2	0.10	0.13	0.13	0.13	0.13
M1–M3	0.22	0.29	0.35	0.21	0.31
M1–M4	0.18	0.22	0.14	0.14	0.20
M1–M5	0.21	0.21	0.22	0.22	0.29
M1–M6	0.19	0.17	0.22	0.20	0.28
M2–M3	0.13	0.22	0.08	0.08	0.12
M2–M4	0.14	0.08	0.12	0.08	0.14
M2–M5	0.07	0.09	0.10	0.13	0.10
M2–M6	0.12	0.27	0.08	0.17	0.08
M3–M4	0.11	0.15	0.11	0.11	0.13
M3–M5	0.16	0.12	0.16	0.09	0.16
M3–M6	0.11	0.12	0.15	0.10	0.14
M4–M5	0.14	0.15	0.11	0.12	0.13
M4–M6	0.13	0.12	0.11	0.11	0.11
M5–M6	0.17	0.17	0.14	0.16	0.15

CASE STUDY

For all five macaque datasets, the optimal model selected by AIC_c was Model 7 (Fig. 1C), with over 99% of the posterior probability centered on this model for each dataset, with the remaining model posterior probabilities were effectively zero for all other models considered (Tables 2, S2–S5). Additionally, the 183 × 183 raw coordinate data the juvenile (M1 erupted) dataset (Table S6) also returned Model 7 as the unambiguously best-supported model. Model 7 can thus be considered the single optimal model describing the pattern of cranial integration in the macaque dataset (Edwards 1992; Royall 1997; Burnham and Anderson 2002).

Model 7 is based on Cheverud's primate-specific six-module structure (Cheverud 1982), proposing distinct within-module ρ′s for all six modules, as well as separate ρ′s for all possible across-module comparisons (total of 22 estimated parameters). All other model structures, including those that proposed no modularity, a neurocranial/facial module structure, more than six cranial modules, or nonprimate-specific module structures, received no support.

Estimated values for ρ were similar for each of the 21 model parameters across the four datasets (Table 3), with very strongly integrated anterior modules (Modules 1 and 2, corresponding to the anterior dentition and nasal/facial bones) and a moderately integrated occipital region (Module 6). Other modules, corresponding to the basicranium, neurocranium, and palatal/molar region were less well integrated, as were intermodule correlations. This is in approximate agreement with previous analyses of integration patterns in mammalian crania (Goswami 2006a).

SUBSAMPLING ANALYSIS

For the subsampling analyses, the unambiguously best-supported model (posterior probabilities > 0.95) was the same as for the full dataset (Model 7) 100% of the time, for the rarefaction to 25 specimens. With 15 specimens, the same model was selected in 48 of 50 analyses. In the two cases of mismatch, Model 7 was one of three top models (posterior probability > 0.05), sharing support with alternative parameterizations of the same Cheverud six-module structure. Subsampling to 10 specimens recovered Model 7 in 36 of 50 runs. In three of the remaining runs in which it was not the best fit model, it was selected as one of the top models (> 0.05 posterior probability), in all cases along with alternative parameterizations of the Cheverud six-module structure. For 11 runs, Model 7 had a posterior probability < 0.05. Thus, even at $n = 10$, this method was successful at identifying the correct model as having a significant posterior probability 78% of the time. Moreoever, of the 14 cases where Model 7 was not the top model, the best-supported model was a variation on the Cheverud model in 12 cases. In only two of the 50 runs was the top model unrelated to Model 7; thus, a relevant model structure, if not the correct parameterization, was recovered in 96% of cases at $n = 10$.

Table 4. Mean optimal values of ρ within the six modules and for the 15 intermodule correlations estimated in Model 7 for the subsampled subadult macaque datasets (reduced to $n = 25$, 15, and 10), compared to the original dataset ($n = 48$).

	$n = 48$	$n = 25$	$n = 15$	$n = 10$
Module 1	0.43	0.48	0.49	0.51
Module 2	0.81	0.80	0.79	0.80
Module 3	0.4	0.42	0.43	0.46
Module 4	0.14	0.20	0.21	0.23
Module 5	0.14	0.16	0.18	0.20
Module 6	0.3	0.32	0.32	0.33
M1–M2	0.13	0.14	0.16	0.19
M1–M3	0.35	0.35	0.36	0.40
M1–M4	0.14	0.17	0.19	0.21
M1–M5	0.22	0.24	0.25	0.27
M1–M6	0.22	0.22	0.24	0.25
M2–M3	0.08	0.11	0.14	0.18
M2–M4	0.12	0.13	0.15	0.18
M2–M5	0.1	0.12	0.13	0.17
M2–M6	0.08	0.10	0.14	0.17
M3–M4	0.11	0.13	0.16	0.18
M3–M5	0.16	0.18	0.20	0.22
M3–M6	0.15	0.16	0.18	0.20
M4–M5	0.11	0.14	0.16	0.19
M4–M6	0.11	0.13	0.15	0.18
M5–M6	0.14	0.15	0.18	0.20

Mean values are averaged over 50 randomly subsampled datasets and demonstrate generally slight increases in magnitude but overall high similarity to original values even at very low sample sizes.

Reconstructed ρ values were consistently very similar to those of the full dataset (Table 4), even at $n = 10$, with mean deviations from ρ values for the full dataset of 0.020 for $n = 25$, to 0.037 for $n = 15$, and 0.062 for $n = 10$. SDs of reconstructed ρ values were similarly low, but unsurprisingly increasing with decreasing sample sizes: 0.023 for $n = 25$, 0.036 for $n = 15$, and 0.042 for $n = 10$. Thus, these further analyses provide strong support that this method is remarkably robust to quite low sample sizes.

Discussion

Extensive simulations varying model complexity, magnitude of mean within-module correlation, and SD of correlations demonstrates that this method is robust under biologically realistic conditions. It performs exceedingly well (perfectly, in fact), when correlations are tightly grouped around hypothetical values of ρ (low SD simulations), regardless of whether the simulated structure is highly modular or entirely lacks any modular structure. With increased dispersion around the ρ values (higher SDs), this method is robust under most conditions, but struggles with highly integrated structures, specifically those that combine two biologically unlikely situations: (1) complete lack of modularity and (2) uniformly and, in most cases, unrealistically high correlations. Only in the case of very high within-module correlations (mainly $\rho = 0.90$, but also involving $\rho = 0.70$ in the no-modularity model and in the high-correlation complex two-module model) does the method return incorrect model structures with high posterior probability. Observing such high correlations, uniformly across all modules or an entire structure is unusual. Previous studies (Conner et al. 2014) have shown that vertebrates, plants, and hemimetabolous insects display mean phenotypic correlations among traits ranging from 0.35 to 0.5, although mean correlations among traits in holometabolous insects may be much higher (~0.84). In the case study presented here, only a single module (Module 2) shows mean within-module correlations >0.7 (Table 3), whereas all other modules are in the moderate to low range of within-module correlations used in these simulations. Our simulations also show that this method is extremely robust in identifying complex models of modularity in which some modules have high within-module correlations and others have moderate or low within-module correlations. Thus, outside of the unusual conditions noted above, our method proves to work with high efficacy, and the few cases of "failure" in conditions typically encountered in most biological systems involved selection of a differently parameterized version of the same model structure.

We further note that no other method currently available for confirmatory analysis of modularity directly compares models of modularity against a model of total integration (e.g., Marquez 2008; Klingenberg 2009; Adams 2016). For example, in the description of the covariance ratio metric, the author provided the important cautionary note that covariance ratio analysis be used only for evaluating patterns of modularity and suggested that Partial Least Squares analysis (Rohlf and Corti 2000; Adams and Felice 2014) be used to evaluate hypotheses of integration (Adams 2016). EMMLi thus provides unprecedented ability to evaluate models of total integration as well as models of modularity, but struggles with correctly identifying the lack of modularity when both SDs of correlations and mean correlations are high. For this reason, we urge caution in interpreting results if the returned posterior probabilities of the best fit models are low (< 0.50), if reconstructed correlations are exceptionally high (uniformly > 0.70), or if multiple unrelated models are returned with posterior probability > 0.05, particularly if SDs of within-module correlations are high. Under those circumstances, we follow Adams (2016) in suggesting that it may prove useful to employ Partial Least Squares analysis to evaluate the support for a highly integrated structure. We further advise users to consider and report all models with posterior probabilities > 0.05.

With regard to the macaque case study, for all five datasets, >99% of the posterior probability distribution was explained by

Model 7, the most parameterized version of Cheverud's model of six cranial modules. This result indicates very strong support for this model of cranial modularity in macaques. Cheverud's (1982) model structure was based on analysis of correlations among interlandmark distances (length measurements) from a dataset of 462 rhesus macaques (*Macaca mulatta*). Cheverud (1982) identified support for this model by calculating an agreement statistic between the hypothesized *F*-sets and empirical *P*-sets, the latter derived by cluster analysis of interlandmark distances in principal component space. This model structure has subsequently tested using theoretical matrix correlation analysis and RV coefficient analysis, with the present Japanese macaque dataset (*M. fuscata*; Goswami and Polly 2010). However, that study also tested two alternative models: the two-module facial/neurocranial model (Models 2–3 in Table 1), and an alternative six-module structure (the "Goswami" models, Models 8–11 in Table 1), based on general patterns of integration among therian mammals (Goswami 2006a). In that study, model selection was not directly possible, as RV coefficient analysis makes no specific hypothesis regarding model parameterization beyond the total number of modules, and theoretical matrix correlation analysis simply compares the correspondence between two matrices, usually with a permutation test to assess support. All three model structures were supported at $P < 0.01$ using theoretical matrix correlation analysis with Mantel's test, although it should be noted that Cheverud's model showed the highest correlations with the empirical data. In the RV coefficient analyses, the two-module model was supported in three of the five datasets ($P < 0.05$), the Goswami model was supported in two of five datasets, and the Cheverud model supported in three of the five datasets, and, where supported, the Cheverud model received the strongest support ($P < 0.001$). However, it was not supported for either adult dataset, whereas both the two-module and the Goswami models received support for the adult male dataset.

The Goswami and Polly (2010) analysis highlighted an important issue with the existing range of confirmatory approaches to analyzing modularity: the lack of a clear way to compare among models across proposing fundamentally different structures of modularity/integration. One can compare the Cheverud six-module model to the Goswami six-module model with RV coefficient analysis, as they both are based on six cranial modules, yet neither can be meaningfully compared to the two-module neurocranial/facial model (Fig. 1). Moreover, there are a range of possibilities, from unintegrated traits within a partially modular structure to entirely different modular structures, that are biologically interesting and potentially informative, but which are impossible to approach with the existing methods.

The results presented here demonstrate the unambiguous support for Cheverud's structure of phenotypic modularity for the macaque cranium, with distinct within- and among-model correlation values. Here, we used maximum likelihood analysis of congruence coefficients derived from multidimensional vector variables, as well as the more standard individual coordinate correlations for one dataset. We focused on trait correlation matrices, rather than variance-covariance matrices, in this method, as the relationships among traits, and not their individual variances, are the primary concern in studies of phenotypic integration and modularity (Olson and Miller 1951; Olson and Miller 1958; Pavlicev et al. 2009; Goswami and Polly 2010; Conner et al. 2014). Benefits of the model selection approach employed here include: (1) the ability to directly compare models of different complexities (such as two- and six-module models) or models of similar complexity, which do not constitute nested subsets of one another (such as the Cheverud (1982) and Goswami (2006a) six-module models), (2) increased precision in model description, in terms of varying numbers of within- and between-module values for ρ; and (3) expansion to mixed models, in which a structure can include both modules and unintegrated traits (e.g., models 20–31 in Table 1).

As noted above, there is an existing method to compare competing models of variational modularity using subspace analysis (Marquez 2008). As with the maximum likelihood approach described here, subspace analysis is a remarkably flexible approach that accurately reflects the complexity of biological systems and is capable of comparing hundreds of models (and indeed performs better with more models).

Both subspace analysis and EMMLI can test multiple variations on a basic model structure, allow for combined or overlapping modules, and conduct direct comparison of models with similar or different parameterizations. In contrast to maximum likelihood analysis as implemented in EMMLi, subspace analysis creates a specific hypothetical covariance matrix for each matrix that fixes between-module covariances at zero. This is rarely the case in biological systems, particularly in proximal modules, and therefore oversimplifies the apparent hierarchical pattern of modularity in systems such as the cranium. The maximum likelihood-based approach described here could be considered preferable because it does not assign an a *priori* value to between-module correlations, and by returning all estimated ρ values for the best-supported model(s), allows for direct assessment of every within- and between-module correlation, which can inform on alternative model structures to test (e.g., if two modules show a between-module ρ equal or similar to their respective within-module ρ values, one could add an additional model that unites those modules into a single grouping).

The two methods also differ on the method of model selection. As a measure of goodness of fit between the observed and model covariance matrices, subspace analysis as implemented in MINT (Marquez 2008) uses γ, and corrects for differences in the parameterizations of each model by regressing γ against the

number of zero elements in each model, generating γ^*, with significance evaluated against expectations from random covariance matrices. To strengthen the evaluation of model rank, a jackknifing approach was used, with model support reflecting how often a model ranked first in the jackknifed samples. The method described here does not require fixing any values, but instead provides an overall model structure and searches for values of ρ that return the maximum likelihood for that structure. The complexity of the model, and correction for the goodness of fit or model selection, is a function of the number of independent estimates of ρ, rather than the number of zero elements in the model.

Because subspace analysis as implemented in MINT has never been developed for 3-D data, we did not conduct a direct comparison of these two methods. Qualitative comparison of the simulations of subspace analysis (Marquez 2008) and those described here suggest that the maximum likelihood approach is more robust to sample size, number of models, model complexity, and magnitude of integration, as well as being available for use with any morphometric dataset. Nonetheless, subspace analysis represented a major improvement on existing methods, and there are numerous interesting aspects to subspace analysis as implemented in MINT, such as the heuristic modeling of additional hypotheses of modularity and the construction of consensus models, both of which could be developed as exploratory tools within a likelihood framework.

In addition to the possibility of incorporating aspects of the Marquez (2008) method, which was developed for the same purpose as the maximum likelihood method described here, there is also vast potential for combining with methods developed for different goals. For example, the Reimmanian spaces for covariance matrices and the distances therein provide a framework for comparing the relative likelihood of one covariance matrix to that of another (Bookstein and Mitteroecker 2014) and could be combined with the method we describe here. In whatever combination, all of these methods are beginning to fill an important need for approaches that are more flexible to the biological reality of complex anatomy.

These benefits are important, as many studies of phenotypic modularity to date have either assumed a hypothesized set of modules without explicitly testing its validity for the taxon of interest (e.g., applying the Cheverud model to other mammals, as in Marroig et al. 2009; Porto et al. 2009), or have tested a single model in the absence of comparison to other potential models, regardless of the support for that one model (e.g., Klingenberg and Marugan-Lobon 2013). Ongoing analyses of other groups suggest that the Cheverud model does not adequately describe all mammalian taxa. For example, EMMLi analysis of a 55 landmark dataset for the red fox, *Vulpes vulpes* (Table S7) recovered the 22-parameter version of the Goswami six-module model as the unambiguous best fit model (for details of dataset, see Goswami 2006b). This result is perhaps unsurprising, as that model was initially based on cluster analyses of a comparative dataset that included a large sample of carnivorans (Goswami 2006a). However, it underscores the flexibility of the model selection approach advocated here, in that many different proposed model structures can be simultaneously compared. The approach implemented in EMMLi, and its many possible future extensions, provides the ability to directly compare diverse hypotheses on the evolution of modularity and integration, which will become increasingly crucial as we drift further from well-established model systems. Further work along these lines will be crucial to identifying where shifts in modularity occur in the tree of life, and what the consequences of those shifts may be for the morphological evolution.

With respect to cranial modularity in macaques, the results from maximum likelihood analyses as implemented in EMMLi underscore two important biological points: (1) the model of two cranial modules based on a neurocranial and a facial module is not supported when compared with more complex six-module hypotheses, and (2) the eight-module structure, although biologically plausible, is not supported. This implies that although a functional model of a facial (masticatory) versus neurocranial organization of the skull is too simplistic to describe phenotypic integration, there is also likely an upper limit to the complexity of cranial integration in the macaque system. In addition, because Model 7 is highly supported in the infant, juvenile, and subadult datasets in addition to the two adult datasets, this pattern of morphological integration appears to be established very early in postnatal ontogeny in *Macaca*. This consistency through ontogeny confirms the previous analyses of this dataset (Goswami and Polly 2010), which suggested that, although relative level of integration decreases through ontogeny, the overall pattern is conserved from infancy to adulthood.

Conclusions

The study of phenotypic modularity has seen rapid growth in recent years. New empirical studies are expanding the topic beyond model systems through development (Young 1959; Zelditch 1988; Hallgrimsson et al. 2004; Zelditch et al. 2006; Goswami et al. 2009; Hallgrimsson et al. 2009; Zelditch et al. 2009; Sears et al. 2012), across the tree of life (Armbruster et al. 2004; Young and Hallgrimsson 2005; Goswami 2006a, b; Goswami 2007; Bell et al. 2011; Bennett and Goswami 2011; Armbruster et al. 2014; Conner et al. 2014; Goswami et al. 2014), and even into the distant past (Goswami 2006a; Bell et al. 2011; Gerber and Hopkins 2011; Webster and Zelditch 2011a, b; Maxwell and Dececchi 2012; Meloro and Slater 2012; Gerber 2013; Goswami et al. 2015). Alongside this extension of taxonomic and temporal sampling, there has been an expansion of analytical tools for the evaluation of modularity and integration. Confirmatory approaches, in

particular, have received much attention in recent years, with RV coefficient analysis in particular being heavily applied to the analysis of modularity. However, these approaches by and large are limited to the direct comparison of models with similar complexities and do not allow for mixed models, where some traits are highly integrated and others are not. The issues caused by these weaknesses in the existing approaches will become increasing problematic as workers diverge from well-studied models into new systems without well-established a priori hypotheses of trait relationships.

Here, we have presented a maximum likelihood and model selection approach to the evaluation of modularity, which can directly compare highly complex hypotheses of trait relationships, including comparisons of nested and non-nested models. We demonstrate this approach using multidimensional vector correlation matrices for a large dataset of macaque crania, confirming the results of previous analyses, but allowing, for the first time, robust discrimination of alternative models. Our results support a highly parameterized model of six cranial modules, with distinct levels of integration within modules, as well as between pairs of modules. This method is applicable to any metric of trait relationship, given the availability of an appropriate transformation, has appropriate Type I error rates, is robust to low sample sizes, and should be incorporated into the existing toolbox for the study of phenotypic modularity in diverse systems.

ACKNOWLEDGMENTS

We thank Prabu Sivasubramaniam and Tim Lucas for development of the R code for EMMLi. Data were gathered at the Primate Research Institute in Inuyama, Japan, with funding provided by the Japanese Society for the Promotion of Science HOPE grant to AG. We thank M. Takai for his role in encouraging and facilitating the research trip to PRI. We thank D. Adams, P.D. Polly, E. Sherratt, C. Klingenberg, UCL's ADaPTiVE laboratory group, and the NHM-UCL-IC Palaeobiology journal club for relevant discussions and comments on this work. The development of this method was supported by a Leverhulme Trust research grant to AG (RPG 2013-124) and a European Research Council grant (ERC-STG-2014-637171) to AG.

DATA ARCHIVING

R code for EMMLi and test files are available at at http://www.goswamilab.com/#!software/c1cxq. 3-D landmark data for Macaca fuscata specimens are also archived on Dryad, doi:10.5061/dryad.091v0.

LITERATURE CITED

Ackermann, R. R., and J. M. Cheverud. 2000. Phenotypic covariance structure in tamarins (genus *Saguinus*): a comparison of variation patterns using matrix correlation and common principal components analysis. Am. J. Phys. Anthropol. 111:489–501.

Adams, D. C. 2016. Evaluating modularity in morphometric data: challenges with the RV coefficient and a new test measure. Methods Ecol. Evol. 7:565–572.

Adams, D. C., and R. N. Felice. 2014. Assessing trait covariation and morphological integration on phylogenies using evolutionary covariance matrices. PLoS One 9:e94335.

Akaike, H. 1973. Information theory as an extension of the maximum likelihood principle. Pp. 267–281 *in* B. N. Petrov and F. Csaki, eds. Second international symposium on information theory. Akademiai Kiado, Budapest, Hungary.

Armbruster, W. S., C. Pelabon, G. H. Bolstad, and T. F. Hansen. 2014. Integrated phenotypes: understanding trait covariation in plants and animals. Phil. Trans. R. Soc. Lond. B 369:20130245.

Armbruster, W. S., C. Pélabon, T. F. Hansen, and C. P. H. Mulder. 2004. Floral integration, modularity, and accuracy: distinguishing complex adaptations from genetic constraints. Pp. 23–49 *in* M. Pigliucci and K. Preston, eds. Phenotypic integration. Oxford Univ. Press, Oxford, U.K.

Bell, E., B. Andres, and A. Goswami. 2011. Limb integration and dissociation in flying vertebrates: a comparison of pterosaurs, birds, and bats. J. Evol. Biol. 24:286–2599.

Bennett, C. V., and A. Goswami. 2011. Does reproductive strategy drive limb integration in marsupials and monotremes? Mamm. Biol. 76: 79–83.

Bookstein, F. L., and P. Mitteroecker. 2014. Comparing covariance matrices by relative eigenanalysis, with applications to organismal biology. Evol. Biol. 41:336–350.

Burnham, K. P., and D. R. Anderson. 2002. Model selection and multimodel inference: a practical information-theoretic approach. Springer, New York.

———. 2004. Multimodel inference: understanding AIC and BIC in model selection. Sociol. Methods Res. 33:261–304.

Cheverud, J. M. 1982. Phenotypic, genetic, and environmental morphological integration in the cranium. Evolution 36:499–516.

———. 1989. A comparative analysis of morphological variation patterns in the Papionines. Evolution 43:1737–1747.

———. 1995. Morphological integration in the saddle-back tamarin (*Saguinus fuscicollis*) cranium. Am. Nat. 145:63–89.

———. 1996. Developmental integration and the evolution of pleiotropy. Am. Zool. 36:44–50.

Conner, J. K., I. A. Cooper, R. J. L. Rosa, S. G. Perez, and A. M. Royer. 2014. Patterns of phenotypic correlations among morphological traits in plants and animals. Phil. Trans. R. Soc. Lond. B 369:20130246.

De Leeuw, J. 1983. Models and methods for the analysis of correlation coefficients. J. Econom. 22:113–137.

Drake, A. G., and C. P. Klingenberg. 2010. Large-scale diversification of skull shape in domestic dogs: disparity and modularity. Am. Nat. 175:289–301.

Edwards, A. W. F. 1992. Likelihood: expanded edition. The Johns Hopkins Univ. Press, Baltimore.

Feldman, G., A. Hayes, S. Kumar, J. Greeson, and J.-P. Laurenceau. 2007. Mindfulness and emotion regulation: the development and initial validation of the Cognitive and Affective Mindfulness Scale-Revised (CAMS-R). J. Psychopathol. Behav. Assess. 29:177–190.

Fruciano, C., P. Franchini, and A. Meyer. 2013. Resampling-based approaches to study variation in morphological modularity. PLoS One 8:e69376.

Gerber, S. 2013. On the relationship between the macroevolutionary trajectories of morphological integration and morphological disparity. PLoS One 8:e63913.

Gerber, S., and M. J. Hopkins. 2011. Mosaic heterochrony and evolutionary modularity: the trilobite genus *Zacanthopsis* as a case study. Evolution 65:3241–3252.

Goswami, A. 2006a. Cranial modularity shifts during mammalian evolution. Am. Nat. 168:270–280.

———. 2006b. Morphological integration in the carnivoran skull. Evolution 60:169–183.

———. 2007. Phylogeny, diet, and cranial integration in australodelphian marsupials. PLoS One 2:e995.

Goswami, A., W. J. Binder, J. A. Meachen, and F. R. O'Keefe. 2015. The fossil record of phenotypic integration and modularity: a deep-time perspective on developmental and evolutionary dynamics. Proc. Natl. Acad. Sci. USA 112:4891–4896.

Goswami, A., and P. D. Polly. 2010. Methods for studying morphological integration and modularity. Pp. 213–243 *in* J. Alroy and E. G. Hunt, eds. Quantitative methods in paleobiology. The Paleontological Society, Boulder, CO.

Goswami, A., J. B. Smaers, C. Soligo, and P. D. Polly. 2014. The macroevolutionary consequences of phenotypic integration: from development to deep time. Phil. Trans. R. Soc. Lond. B 369:20130254.

Goswami, A., V. Weisbecker, and M. R. Sanchez-Villagra. 2009. Developmental modularity and the marsupial-placental dichotomy. J. Exp. Zool. B 312B:186–195.

Hallgrimsson, B., H. Jamniczky, N. M. Young, C. Rolian, T. E. Parsons, J. C. Boughner, and R. S. Marcucio. 2009. Deciphering the palimpsest: studying the relationship between morphological integration and phenotypic covariation. Evol. Biol. 36:355–376.

Hallgrimsson, B., K. Willmore, C. Dorval, and D. M. L. Cooper. 2004. Craniofacial variability and modularity in macaques and mice. J. Exp. Zool. B 302B:207–225.

Hurvich, C. M., and C.-L. Tsai. 1989. Regression and time series model selection in small samples. Biometrika 76:297–307.

Klingenberg, C. P. 2008. Morphological integration and developmental modularity. Annu. Rev. Ecol. Evol. Syst. 39:115–132.

———. 2009. Morphometric integration and modularity in configurations of landmarks: tools for evaluating a prior hypotheses. Evol. Dev. 11:405–421.

———. 2013. Cranial integration and modularity: insights into evolution and development from morphometric data. Hystrix 24:43–58.

———. 2014. Studying morphological integration and modularity at multiple levels: concepts and analysis. Phil. Trans. R. Soc. Lond. B 369:20130249.

Klingenberg, C. P., and J. Marugan-Lobon. 2013. Evolutionary covariation in geometric morphometric data: analyzing integration, modularity and allometry in a phylogenetic context. Syst. Biol. 62:591–610.

LeBel, E. P., and B. Gawronski. 2009. How to find what's in a name: scrutinizing the optimality of five scoring algorithms for the name-letter task. Eur. J. Pers. 23:85–106.

Marquez, E. J. 2008. A statistical framework for testing modularity in multidimensional data. Evolution 62:2688–2708.

Marroig, G., and J. M. Cheverud. 2001. A comparison of phenotypic variation and covariation patterns and the role of phylogeny, ecology, and ontogeny during cranial evolution of New World monkeys. Evolution 55:2576–2600.

Marroig, G., L. Shirai, A. Porto, F. B. de Oliveira, and V. De Conto. 2009. The evolution of modularity in the mammalian skull II: evolutionary consequences. Evol. Biol. 36:136–148.

Maxwell, E. E., and T. A. Dececchi. 2012. Ontogenetic and stratigraphic influence on observed phenotypic integration in the limb skeleton of a fossil tetrapod. Paleobiology 39:123–134.

Meloro, C., and G. J. Slater. 2012. Covariation in the skull modules of cats: the challenge of growing saber-like canines. J. Vert. Paleontol. 32:677–685.

Olson, E. C., and R. L. Miller. 1951. A mathematical model applied to the evolution of species. Evolution 5:325–338.

———. 1958. Morphological integration. Univ. of Chicago Press, Chicago.

Pavlicev, M., J. M. Cheverud, and G. P. Wagner. 2009. Measuring morphological integration using eigenvalue variance. Evol. Biol. 36:157–170.

Porto, A., F. B. de Oliveira, L. Shirai, V. De Conto, and G. Marroig. 2009. The evolution of modularity in the mammalian skull I: morphological integration patterns and magnitudes. Evol. Biol. 36:118–135.

Rohlf, F. J., and M. Corti. 2000. Use of two-block partial least-squares to study covariation in shape. Syst. Biol. 49:740–753.

Royall, R. M. 1997. Statistical evidence: a likelihood paradigm. Chapman and Hall, New York.

Sears, K. E., C. Doroba, X. Cao, D. Xie, and S. Zhong. 2012. Molecluar determinants of marsupial integration and constraint. Pp. 257–278 *in* R. J. Asher and J. Mueller, eds. From clone to bone: the synergy of morphological and molecular tools in palaeobiology. Cambridge Univ. Press, Cambridge, U.K.

Sokal, R. R., and F. J. Rohlf. 1995. Biometry. W. H. Freeman, New York.

Steiger, J. H. 1980a. Testing pattern hypotheses on correlation matricies: alternative statistics and some empirical results. Multivariate Behav. Res. 15:335–352.

———. 1980b. Tests for comparing elements of a correlation matrix. Psychol. Bull. 87:245–251.

Wager, T. D., D. J. Scott, and J.-K. Zubieta. 2007. Placebo effects on human μ-opioid activity during pain. Proc. Natl. Acad. Sci. USA 104:11056–11061.

Wagner, P. J. 2000. Likelihood tests of hypothesized durations: determining and accommodating biasing factors. Paleobiology 26:431–449.

Webster, M., and M. L. Zelditch. 2011a. Evolutionary lability of integration in Cambrian ptychopariod trilobites. Evol. Biol. 38:144–162.

———. 2011b. Modularity of a Cambrian ptychoparioid trilobite cranidium. Evol. Dev. 13:96–109.

Young, N. M., and B. Hallgrimsson. 2005. Serial homology and the evolution of mammalian limb covariation structure. Evolution 59:2691–2704.

Young, R. W. 1959. The influence of cranial contents on postnatal growth of the skull in the rat. Am. J. Anat. 105:383–415.

Zelditch, M. L. 1988. Ontogenetic variation in patterns of phenotypic integration in the laboratory rat. Evolution 42:28–41.

Zelditch, M. L., J. G. Mezey, H. D. Sheets, B. L. Lundrigan, and J. T. Garland. 2006. Developmental regulation of skull morphology II: ontogenetic dynamics of covariance. Evol. Biol. 8:46–60.

Zelditch, M. L., A. R. Wood, and D. L. Swiderski. 2009. Building developmental integration into functional systems: function-induced integration of mandibular shape. Evol. Biol. 36:71–87.

Associate Editor: D. Adams
Handling Editor: R. Shaw

Supporting Information

Additional Supporting Information may be found in the online version of this article at the publisher's website:

Table S1. Identification of landmarks from the dataset presented in (Goswami and Polly 2010).
Table S2. Results for the Adult Male dataset ($n = 25$) using congruence coefficients.
Table S3. Results for the Adult Female dataset ($n = 24$) using congruence coefficients.
Table S4. Results for the Juvenile (M1 erupted) dataset ($n = 42$) using congruence coefficients.
Table S5. Results for the Infant (deciduous dentition only) dataset ($n = 42$) using congruence coefficients.
Table S6. Results for the Juvenile (M1 erupted) dataset ($n = 42$) using congruence coefficients for individual x-, y-, and z-coordinates.
Table S7. Results for the red fox, *Vulpes vulpes*, adult dataset ($n = 22$) using congruence coefficients for 55 landmarks, detailed in (Goswami 2006b).